

Partial synchronization of relaxation oscillators with repulsive coupling in autocatalytic integrate-and-fire model and electrochemical experiments

Hiroshi Kori,¹ István Z. Kiss,² Swati Jain,³ and John L. Hudson^{3,a)}

¹Department of Information Sciences, Ochanomizu University, Tokyo 112-8610, Japan

²Department of Chemistry, Saint Louis University, St. Louis, Missouri 63103, USA

³Department of Chemical Engineering, University of Virginia, Charlottesville, Virginia 22904, USA

(Received 15 January 2018; accepted 12 March 2018; published online 6 April 2018)

Experiments and supporting theoretical analysis are presented to describe the synchronization patterns that can be observed with a population of globally coupled electrochemical oscillators close to a homoclinic, saddle-loop bifurcation, where the coupling is repulsive in the electrode potential. While attractive coupling generates phase clusters and desynchronized states, repulsive coupling results in synchronized oscillations. The experiments are interpreted with a phenomenological model that captures the waveform of the oscillations (exponential increase) followed by a refractory period. The globally coupled autocatalytic integrate-and-fire model predicts the development of partially synchronized states that occur through attracting heteroclinic cycles between out-of-phase two-cluster states. Similar behavior can be expected in many other systems where the oscillations occur close to a saddle-loop bifurcation, e.g., with Morris-Lecar neurons. *Published by AIP Publishing*. <https://doi.org/10.1063/1.5022497>

Many oscillatory processes underlie the functioning of important biological and engineered systems. The waveform of the oscillation of a variable (e.g., concentration of substances) has strong impact on the overall behavior, e.g., on how the oscillations synchronize together. The waveform can be smooth, nearly sinusoidal, or relaxation type, where slow variations are followed by a quick spike. In this paper, we performed experiments with a chemical oscillatory system, where the waveform had strong relaxation character, and show that such a system, in contrast with the previously studied smooth oscillation, can produce synchronization with repulsive coupling among the variables. The experiments are interpreted with a simple mathematical model, where the relaxation character of the waveform can be tuned to generate complex synchronization patterns.

I. INTRODUCTION

The widespread occurrence of different types of synchronization patterns of nonlinear dynamical systems calls for theoretical description using simplified, generic models.^{1–3} The development of such models depends on local nonlinear features of the oscillating units and the type of interactions. When the interactions are global and weak, the oscillations can often be described with phase models

$$\frac{d\phi_i}{dt} = \omega_i + \sum_{j=1}^N \Gamma(\phi_i - \phi_j), \quad (1)$$

where ϕ_i ($i = 1, \dots, N$) and ω_i are the phase and the natural frequency of the i -th oscillator, respectively, and N is the number of oscillators.² The central component in such a

phase model is the functional form of $\Gamma(\phi)$. For example, close to a Hopf bifurcation with coupling that occurs through an additive term of variable differences, Γ is a sinusoidal function, possibly shifted with a constant term, as in the Kuramoto-Sakaguchi model.² Further away from the Hopf bifurcation, higher harmonics can occur in Z , as theoretically shown,⁴ and observed in many chemical and biological oscillators.^{5–10} Correspondingly, higher harmonics appear also in H giving rise to phase cluster dynamics.⁸ Because of the relative simplicity of the mathematical structure of phase models, very often analytical solutions exist for synchronization patterns.

Many oscillations in nature, for example, in chemistry and neurophysiology, have more complex shapes. The slow, exponential decaying waveform, corresponding to the charging of the membrane potential in biology, motivated the development of integrate-and-fire (IF) types of models. In IF models, after the process is complete, there is a quick, often instantaneous discharge that allows the process to restart. Such models, which typically describe the behavior close to bifurcation [e.g., homoclinic saddle loop (SL) bifurcation or saddle-node bifurcation of infinity period (SNIPER)],¹¹ can generate rich dynamics in networks that include synchronization,¹² asynchronous dynamics,¹³ clustering,¹⁴ or chimera states.¹⁵ Systems close to a SNIPER or SL bifurcation can generate a refractory period: the discharging process is not instantaneous but occurs over a relatively short interval during which the system is insensitive to external perturbations.¹⁶

In this paper, we design an integrate-and-fire type of model for the description of synchronization patterns of an electrochemical oscillator close to SL bifurcation. The experiment performed with a repulsive coupling of a population of electrochemical oscillators exhibited a synchronized state. The extent of the synchronization is investigated as a function of distance from the SL bifurcation. The

^{a)}Deceased.

experiments are interpreted with an autocatalytic integrate-and-fire (AIF) model, adjusted for the exponentially increasing waveform for the experiments. The AIF model is analyzed using a phase model description. The model analysis reveals the type of synchronized oscillations, clusters, and partially synchronized states.

II. EXPERIMENTAL RESULTS AND ANALYSIS

We carried out experiments to explore the synchronization behavior with $N = 64$ electrochemical relaxation oscillators close to a homoclinic bifurcation. The system consists of 64 metal wires; the rate of metal dissolution (currents of the electrodes) at constant circuit potential (U) is measured. The currents of the electrodes become oscillatory through a supercritical Hopf bifurcation point at $U = 1.0$ V; the oscillations are smooth near the Hopf bifurcation point. As the potential is increased further, relaxation oscillations are seen that disappear into a steady state through a homoclinic bifurcation at about $U = 1.31$ V.⁹ The electrodes are coupled with a combination of resistors coupled in series (R_s) and in parallel (R_p); the imposed coupling strength is $K = NR_s/R_p$. Negative coupling was induced with the application of negative series resistance (built in a Princeton Applied Research 273A potentiostat).⁴

In a previous publication,⁴ we showed that close to the Hopf bifurcation with strong negative coupling the weak nonlinearities can generate cluster states. Further away from the Hopf bifurcation, the system showed desynchronized behavior.

Here, we focus on behavior at even larger circuit potentials, where relaxation oscillations occur that cease through a homoclinic bifurcation. Figure 1 shows that under these conditions, the system exhibits nearly synchronized behavior. While the oscillators do not spike completely together [see Figs. 1(a) and 1(c) for time series in current vs time and grayscale plots, respectively], they form a tightly synchronized cluster. This synchronization can be also seen in the

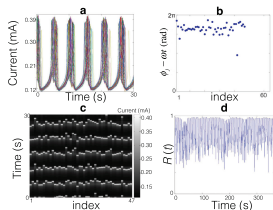


FIG. 1. Experiments: Nearly in-phase synchronization with negative global coupling very close to homoclinic bifurcation. (a) Time series of current oscillations. (b) Phase snapshot. (c) Grayscale plot of currents. (d) Order parameter vs. time. $U = 1.3$ V.

phase snapshot in Fig. 1(b), where the phases of the oscillators, $\phi_i(t)$, were calculated with the Hilbert transform approach.^{3,17} The extent of synchronization can be quantitatively characterized using the average Kuramoto order parameter $\langle R \rangle$,² which is obtained by averaging the order parameter $R(t) = \frac{1}{N} |\sum_{j=1}^N e^{i\phi_j(t)}|$ after a transient. We have $R(t) = 1$ when all the phases take the same value (in-phase synchrony) and $R(t) = 0$ for a uniform phase distribution including the balanced cluster states. As shown in Fig. 1(d), the synchronized oscillations generate large order parameter close to 1.

We carried out a series of experiments in which the circuit potential was increased and the averaged Kuramoto order was calculated (see Fig. 2). As the circuit potential of the oscillators was increased, an increase in the Kuramoto order parameter was observed. Interestingly, the increase in the order is not very sharp, as, for example, could be expected from a bifurcation that leads to a stable one-cluster state. In the inset, it is shown that at $U = 1.25$ V, in the state space an enhanced synchronization is present.

A. Phase model analysis with experimentally obtained phase interaction function

For better experimental characterization of the synchronization transition with increasing the circuit potential, we performed a phase model analysis, where the phase interaction function was constructed from Refs. 9 and 18. Using the phase model, the stability of the different cluster states can be calculated for a population of globally coupled oscillators. For a large interval in the moderately relaxational oscillation region ($1.25 \text{ V} < U < 1.28 \text{ V}$), the experimentally measured interaction function predicted desynchrony; however, a one cluster state with elevated value of order parameter was experimentally observed (see Fig. 2).

The difference between a population generating low and elevated $\langle R \rangle$ can be demonstrated with experimentally determined coupling functions for $U = 1.225$ V and $U = 1.265$ V.^{9,18} The measured $\Gamma(\phi)$ functions were expressed as a Fourier series up to tenth harmonics, which are shown in Fig. 3(a). By directly simulating the phase model with these $\Gamma(\phi)$ functions, we obtained dynamics similar to experimental ones, as shown in Figs. 3(b) and 3(c). Further using the $\Gamma(\phi)$ functions, we

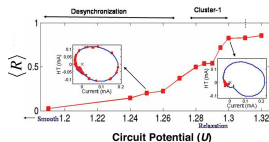


FIG. 2. Experiments: Emerging order with approaching saddle loop bifurcation point by increasing the circuit potential, U . The distribution of elements, in the Hilbert transform space, at $U = 1.25$ V is shown in the left side. The distribution of elements in a synchronized state at $U = 1.3$ V is shown in right side.

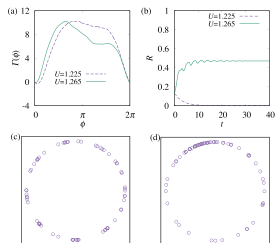


FIG. 3. Numerical results using the phase model with experimentally measured coupling function. (a) Phase interaction function measured experimentally for $U = 1.225$ V and $U = 1.265$ V. (b) Time-series of the order parameter $R(t)$. (c) and (d) Snapshots of the phases at $t = 40$ for $U = 1.225$ V and $U = 1.265$ V, respectively. The same random initial condition was employed both for $U = 1.225$ V and $U = 1.265$ V.

checked the linear stability (see Appendix A) of the balanced n -cluster states ($n = 1, \dots, 10$),¹⁹ indicating that the states with $n = 7, 8$, and 9 are stable for $U = 1.225$ V, whereas no state is stable for $U = 1.265$ V. The former result explains the almost uniform distribution of phases observed for $U = 1.225$ V. However, the latter cannot account for the emergence of a type of one cluster state observed for $U = 1.265$ V. In order to explore the emergent collective synchronization approaching the homoclinic bifurcation, we develop a phenomenological model in Sec. III.

III. AUTOCATALYTIC INTEGRATE-AND-FIRE MODEL

A. Model

We construct a simple, one-dimensional model for oscillators close to a homoclinic bifurcation. This model is motivated by the waveform of many chemical and biological oscillators composed of an “excitatory” phase with exponential increase followed by a usually sharp decrease with a refractory period, as observed in Fig. 1(a). Therefore, a coupled oscillator is described by

$$\frac{dv}{dt} = v + Kp(t), \quad (2)$$

where $v = v(t)$ is the state variable, K is the coupling strength, and $p(t)$ is an external input describing the influence from other oscillators.

When v reaches 1, its value is smoothly reset to parameter a ($0 < a < 1$) by obeying

$$v = e^{-b(t-t_{\text{fire}})}, \quad (3)$$

where t_{fire} is the latest time at which v becomes 1. Here, we have assumed that the oscillator is not influenced by other

oscillators (or external forces) during the resetting process, i.e., in an absolute refractory period. A typical time series in the absence of coupling (i.e., $K = 0$) is shown in Fig. 4(a). In this model, parameters a and b characterize the intrinsic dynamical property of an oscillator. It is more convenient to characterize the relaxation character of the oscillator by using the excitatory period τ_e and refractory period τ_r , given by

$$\tau_e = -\ln a, \quad (4)$$

$$\tau_r = -\frac{\ln a}{b}. \quad (5)$$

For convenience, we denote the intrinsic period by

$$T = \tau_e + \tau_r. \quad (6)$$

Larger τ_e values compared to τ_r indicate stronger relaxation character and closer distance to the homoclinic bifurcation (at which τ_e becomes infinite).

B. Phase reduction

As a coupled oscillator system, we consider

$$\frac{dv}{dt} = v + K(v' - v), \quad (7)$$

where $v'(t)$ describes the state of an interacting oscillator. The coupling term $K(v' - v)$ describes diffusive coupling. In the context of electrochemical and neural dynamics, v and K describe the electric potential and the conductance, respectively. Although we have included only one interacting oscillator described by v' in Eq. (7) for simplicity, we can consider a network of interacting oscillators by replacing $v' - v$ with $\sum_j (v_j - v)$, where v_j are the state variables of interacting oscillators.

The phase model corresponding to this model can be calculated analytically. We first define the phase $\varphi(v(t))$ as a function of the state $v(t)$ such that $\frac{d}{dt}\varphi(v(t)) = 1$ for $K = 0$, i.e.,

$$\varphi(v) = \begin{cases} \ln v + \tau_e & (0 \leq \varphi < \tau_e, \text{excitatory phase}), \\ -\frac{\tau_r}{\tau_e} \ln v + \tau_e & (\tau_e \leq \varphi < T, \text{refractory phase}). \end{cases} \quad (8)$$

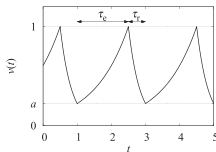


FIG. 4. Typical waveform of the AIF oscillator. $\tau_e = 1.5$, $\tau_r = 0.5$.

By solving reversely, we obtain

$$v(t) = \bar{v}(\varphi(t)), \quad (9)$$

where

$$\bar{v}(\varphi) = \begin{cases} e^{\varphi - \tau_c} & (0 \leq \varphi < \tau_c), \\ e^{-\frac{\tau_c}{T}(\varphi - \tau_c)} & (\tau_c \leq \varphi < T). \end{cases} \quad (10)$$

We now derive the dynamical equation of $\varphi(t)$. For the excitatory phase, using $\frac{d\varphi}{dt} = \frac{d\varphi}{dt} \frac{dt}{d\varphi}$ with Eqs. (2) and (9), we obtain

$$\frac{d\varphi}{dt} = 1 + K\bar{Z}(\varphi)\{\bar{v}(\varphi') - \bar{v}(\varphi)\}, \quad (11)$$

where $\bar{Z}(\varphi) = e^{\varphi - \tau_c}$ and $\varphi'(t)$ is the phase of the state $v'(t)$. For the refractory phase, we have $\bar{v}(\varphi) = 1$. Altogether, we obtain Eq. (11) with \bar{Z} redefined as

$$\bar{Z}(\varphi) = \begin{cases} e^{\varphi - \tau_c} & (0 \leq \varphi < \tau_c), \\ 0 & (\tau_c \leq \varphi < T). \end{cases} \quad (12)$$

For $K \ll 1$, we may further reduce Eq. (11) to a more tractable equation, given as

$$\dot{\varphi} = 1 + K\bar{\Gamma}(\varphi - \varphi'), \quad (13)$$

where the coupling function $\bar{\Gamma}$ is obtained by averaging the right hand side of Eq. (11) over the period T ,² i.e.,

$$\bar{\Gamma}(\varphi) = \frac{1}{T} \int_0^T \bar{Z}(\varphi + \theta) \{\bar{v}(\theta) - \bar{v}(\varphi + \theta)\} d\theta. \quad (14)$$

For $\tau_c > \tau_r$, which we assume henceforth, we obtain

$$\bar{\Gamma}(\varphi) = \begin{cases} [\Gamma_1(\varphi) - \tau_c]/T & \text{for } 0 \leq \varphi < \tau_r, \\ [\Gamma_2(\varphi) - \tau_c]/T & \text{for } \tau_r \leq \varphi < \tau_c, \\ [\Gamma_3(\varphi) - \tau_c]/T & \text{for } \tau_c \leq \varphi \leq T, \end{cases} \quad (15)$$

where

$$\Gamma_1(\varphi) = \frac{\tau_r}{T} e^{\frac{\tau_r}{T}\varphi} + \left(-\varphi + \tau_c - \frac{\tau_r}{T}\right) e^{-\varphi}, \quad (16)$$

$$\Gamma_2(\varphi) = \left(\varphi - \tau_r + \frac{\tau_r}{T}\right) e^{\tau_r - \varphi} + \left(-\varphi + \tau_c - \frac{\tau_r}{T}\right) e^{-\varphi}, \quad (17)$$

$$\Gamma_3(\varphi) = \left(\varphi - \tau_r + \frac{\tau_r}{T}\right) e^{\tau_r - \varphi} - \frac{\tau_r}{T} e^{-\frac{\tau_r}{T}(T - \varphi)}. \quad (18)$$

Alternatively, by introducing the phase ϕ ($0 \leq \phi < 2\pi$) as

$$\phi = \omega\varphi, \quad (19)$$

where $\omega = \frac{2\pi}{T}$, we obtain

$$\dot{\phi} = \omega + K\Gamma(\phi - \phi'), \quad (20)$$

where

$$\Gamma(\phi) = \omega \bar{\Gamma}\left(\frac{\phi}{\omega}\right). \quad (21)$$

For both Eqs. (13) and (20), $|K|$ values only determine the time scale, thus we may set $K = 1$ or $K = -1$ for positive and negative coupling, respectively, without loss of generality. In Fig. 5, we show typical $Z(\varphi)$ and $\Gamma(\phi)$ functions. There is a notable similarity between $\Gamma(\phi)$ functions obtained experimentally and theoretically [Figs. 3(a) and 5(c)]. In particular, there is a rapid growth in a region of small ϕ , and the slope is steeper for a more relaxation oscillator, i.e., higher U and τ_c values.

C. Analysis

Now, we analyze a system of globally coupled oscillators. The system is given as

$$\dot{v}_i = v_i + \frac{K}{N} \sum_{j=1}^N (v_j - v_i), \quad (22)$$

and its corresponding phase model is obtained as

$$\dot{\phi}_i = \omega + \frac{K}{N} \sum_{j=1}^N \Gamma(\phi_i - \phi_j), \quad (23)$$

where v_i and ϕ_i ($i = 1, \dots, N$) are the state and phase of oscillator i , respectively. As described in Appendix A, the local stability of the balanced n -cluster states is determined by the nontrivial maximum eigenvalue.¹⁹ Figure 6 shows a stability diagram. Here, we only consider $n \leq 10$ for simplicity. With positive coupling ($K > 0$), at low values of τ_c only the 1-cluster state is stable. As the relaxation character increases, 2, 3, 4-cluster states become progressively stable. With negative coupling, stable cluster states exist for small τ_c values. However, all cluster states are predicted to be unstable for large τ_c values. Numerical simulations with the AIF model indicate that the average Kuramoto order parameter (R) is vanishingly small for small τ_c values. There, in accordance with the stability analysis, balanced cluster states were observed. However, R begins to increase at $\tau_c \approx 2.0$ and takes a large value (close to unity) as τ_c increases.

To understand the emergence of synchrony, we first focus on its onset at $\tau_c \approx 2.0$. As shown in Fig. 6(b), only the balanced 7-cluster state is stable just below $\tau_c = 2.0$ and the state loses stability at $\tau_c \approx 2.0$. As also indicated in Fig. 6(b),

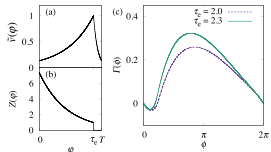


FIG. 5. Functions in the AIF model. (a) Waveform $\bar{v}(\varphi)$. (b) Phase sensitivity function $Z(\varphi)$. (c) Phase interaction functions $\Gamma(\phi)$. $\tau_c = 2.0$ in (a) and (b), and $\tau_c = 0.3$.

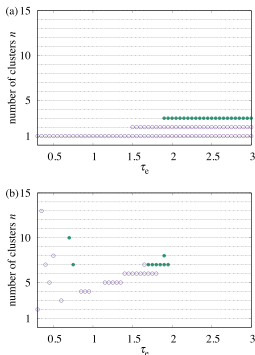


FIG. 6. Stability diagram for the AIF system with global coupling. (a) Positive coupling. (b) Negative coupling. Each circle indicates that the n -cluster state is stable at the τ_c value. Open and filled circles indicate that the largest nontrivial eigenvalue is a real and imaginary value, respectively.

the maximum nontrivial eigenvalue is imaginary and its mode is associated with inter-cluster fluctuations (see Appendix A). This implies that the balanced 7-cluster state loses its stability through a Hopf bifurcation and the distribution of relative phases $\phi_j - \phi_1$ starts to oscillate after that. Figure 8 shows the time series of relative phases for different τ_c values. At $\tau_c = 1.8$ [Fig. 8(a)], the system converged to the balanced 7-cluster state from a random initial condition, as predicted. At $\tau_c = 2.0$ [Fig. 8(b)], where no balanced cluster states are predicted to be stable, the system converged to a slightly scattered balanced cluster state, in which relative phases between clusters oscillate with time. This state can be interpreted as a similar state to those that bifurcate from the balanced n -cluster states via Hopf bifurcations.

For larger τ_c values, no well-defined clusters are observed. Instead, the oscillators form a noisy cloud similar to Fig. 3(d) in spite of the instability of the one-cluster state. Figure 8(c) shows a typical time series of relative phases, where the center of the cloud travels with time like a wave, i.e., each oscillator enters and exits from a cloud repeatedly. When τ_c is further increased, $\langle R \rangle$ suddenly jumps at $\tau_c \approx 2.8$, as shown in Fig. 7. Figure 8(d) shows typical time series of relative phases for $\tau_c > 2.8$. The oscillators split into two groups, and each group repeats aggregation and breakup. Such a phenomenon is referred to as “slow switching,” as the system slowly switches back and forth between a pair of two cluster states.^{14,20,21} This phenomenon occurs, because there

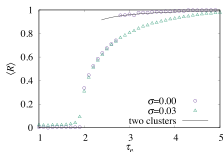


FIG. 7. Average order parameter $\langle R \rangle$ versus τ_c in the AIF system ($N=64$) with negative coupling for noiseless ($\sigma=0.00$) and noisy ($\sigma=0.03$) systems. The solid curve shows predicted $\langle R \rangle$ values, given by Eq. (24).

are attracting heteroclinic cycles between pairs of unstable out-of-phase two-cluster states. The condition for the existence of attracting heteroclinic cycles is obtained through the stability analysis of the two-cluster states that are different from the balanced two-cluster states (see Appendix B). As a result, we find that the attracting heteroclinic cycles exist in our AIF system for large τ_c values. If the system converges to such a cycle, $\langle R \rangle$ is well approximated by

$$\langle R \rangle \approx \sqrt{\frac{1 + \cos \Delta\phi}{2}}, \quad (24)$$

where $\Delta\phi$ is the phase difference between two clusters. $\Delta\phi$ is obtained as the solution to $\Gamma(\Delta\phi) = \Gamma(-\Delta\phi)$ (see Appendix B), which is typically small, e.g., $\Delta\phi \approx 0.3$ rad at $\tau_c = 0.3$, thus high $\langle R \rangle$ values are predicted. In Fig. 7, predicted $\langle R \rangle$ values are plotted as the solid curve, which is in a good agreement with numerical $\langle R \rangle$ values for $\tau_c > 2.8$. This result indicates that the heteroclinic cycles become attracting at $\tau_c \approx 2.8$. When heteroclinic cycles are nonattracting, it

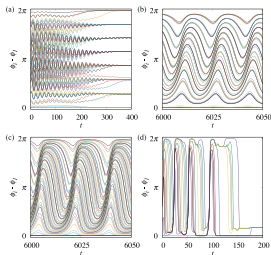


FIG. 8. Time series of phase differences $\phi_j - \phi_1$ of the AIF system. (a) $\tau_c = 1.90$. (b) $\tau_c = 2.00$. (c) $\tau_c = 2.20$. (d) $\tau_c = 3.30$. $N=64$ except (d), where $N=10$ for better visibility.

can be generally expected that attracting limit-cycles exist close to the heteroclinic cycles. Actually, the phenomenon shown in Fig. 8(d) is rather similar to that in Fig. 8(c), in particular, before the system gets very close to two cluster states (e.g., $t \approx 50$). Thus, our interpretation of noisy one-cluster state is a noisy dynamics along heteroclinic cycles between unstable, saddle type cluster states.

We also investigate the effect of noise. We consider

$$\dot{\phi}_i = \omega + \frac{K}{N} \sum_{j=1}^N \Gamma(\phi_j - \phi_i) + \sigma \xi_i, \quad (25)$$

where σ is noise intensity and $\xi_i(t)$ is white Gaussian noise with zero mean and unit variance. The green triangles in Fig. 7 show $\langle R \rangle$ values obtained by numerical simulation of Eq. (25). As seen, $\langle R \rangle$ values are similar to those in the noiseless system for $\tau_c < 2.8$. Effect of noise is significant $\tau_c \geq 2.8$ because noise inhibits the system to get very close to unstable two-cluster states.^{14,20,21} Thus, with noise, the noisy one-cluster state persists even for $\tau_c \geq 2.8$. By a numerical simulation, we confirmed qualitatively that the same result is obtained for nonidentical oscillators [i.e., ω in Eq. (25) is i -dependent]. These results indicate that the noisy one-cluster state is robust against noise. Therefore, we interpret that the noisy one-cluster state observed in the experiment is generated by an itinerant synchronization involving unstable, saddle type cluster states.

IV. CONCLUSION

In summary, we have shown that a noisy synchronized state can occur in a negatively coupled electrochemical oscillator system; this synchronized state was explained theoretically as an itinerant motion among unstable cluster states. This itinerant synchronization could further contribute to the wide range of emergent collective behavior of physical, chemical, and biological oscillators. We expect that similar phenomena can be reproduced in other oscillators when they are close to homoclinic bifurcation. For example, the Belousov-Zhabotinsky oscillatory reaction also exhibits phase response curve similar to the predictions of AIF model.²² Neural models are good candidates as well, because many of them, such as the Morris-Lecar model,¹¹ exhibit homoclinic bifurcation.

Many integrate-and-fire models proposed previously assume instantaneous resetting, which yields discontinuous $r(t)$.^{12,15,21,23,24} In contrast, in the AIF model, we have introduced the resting process with finite period τ_r , which enables us to consider continuous $r(t)$. This feature is not only natural but also a great advantage in mathematical and numerical treatments because then our model has continuous flow at any time. Thereby, delicate problems due to discontinuity can be avoided. For example, it is important that the interaction function $\Gamma(\phi)$ has continuous derivative at $\phi=0$, i.e., $\Gamma'_1(0) = \Gamma'_1(2\pi) = -\tau_c$ for nonvanishing τ_c , because $\Gamma'(0)$ plays a vital role in determining many synchronous states.

ACKNOWLEDGMENTS

H.K. acknowledges supports from MEXT KAKENHI Grant No. 15H05876. I.Z.K. acknowledges support from

National Science Foundation CHE-1465013 grant. One of the authors, H.K., met John Hudson at Fritz Haber Institute in Berlin in 2003 and after that had many occasions to collaborate with him. All of them were great experiences for H.K., through which H.K. learned a lot about how to work on science and enjoy collaborations.

APPENDIX A: STABILITY OF THE BALANCED CLUSTER STATES

We briefly summarize the stability analysis of the balanced cluster states.¹⁹ In the phase model given by Eq. (23), the balanced n -cluster state always exists for any Γ . In the balanced n -cluster state, N/n oscillators make a point cluster and these oscillators take the same phase Φ_k ($k = 0, 1, \dots, n-1$), given by

$$\Phi_k = \Omega t + \frac{2\pi k}{n}, \quad (A1)$$

where Ω is the actual frequency. By substituting Eq. (A1) into Eq. (23), we obtain

$$\Omega = \frac{1}{n} \sum_{k=0}^{n-1} \Gamma\left(\frac{2\pi k}{n}\right). \quad (A2)$$

By solving the eigenvalue problem for the corresponding stability matrix, we obtain N eigenvalues as

$$\tilde{\lambda} = \frac{1}{n} \sum_{k=0}^{n-1} \Gamma\left(\frac{2\pi k}{n}\right), \quad (A3)$$

$$\lambda_p = \frac{1}{n} \sum_{k=0}^{n-1} \Gamma\left(\frac{2\pi k}{n}\right) (1 - e^{-i2\pi k p/n}), \quad (A4)$$

where the former has $N - n$ multiplicity and is associated with intra-cluster fluctuation, and the latter has 1 multiplicity for each p ($p = 0, 1, \dots, n-1$) and is associated with inter-cluster fluctuation. There is one trivial eigenvalue $\lambda_0 = 0$, which is associated with uniform phase shift. The balanced n -cluster state is linearly stable if and only if all the remaining eigenvalues have negative real parts.

The derivative of $\tilde{\Gamma}(\varphi)$ is

$$\tilde{\Gamma}'(\varphi) = \begin{cases} \tilde{\Gamma}'_1(\varphi)/T & \text{for } 0 \leq \varphi \leq \tau_r, \\ \tilde{\Gamma}'_2(\varphi)/T & \text{for } \tau_r \leq \varphi \leq \tau_c, \\ \tilde{\Gamma}'_3(\varphi)/T & \text{for } \tau_c \leq \varphi \leq T, \end{cases} \quad (A5)$$

where

$$\tilde{\Gamma}'_1(\varphi) = \frac{\tau_c}{T} e^{i\varphi} - \left(-\varphi + \tau_c - \frac{\tau_r}{T} + 1\right) e^{-\varphi}, \quad (A6)$$

$$\tilde{\Gamma}'_2(\varphi) = -\left(\varphi - \tau_r + \frac{\tau_r}{T} - 1\right) e^{\tau - \varphi} - \left(-\varphi + \tau_c - \frac{\tau_r}{T} + 1\right) e^{-\varphi}, \quad (A7)$$

$$\tilde{\Gamma}'_3(\phi) = -\left(\phi - \tau_r + \frac{\tau_r}{T} - 1\right)e^{T-\phi} - \frac{\tau_c}{T}e^{-\frac{\tau_c}{T}(T-\phi)}. \quad (\text{A8})$$

$$\text{Note } \Gamma'(\phi) = \frac{d\phi}{d\phi} \frac{d\phi}{d\phi} (\omega \tilde{\Gamma}(\phi)) = \tilde{\Gamma}'\left(\frac{\phi}{\omega}\right).$$

APPENDIX B: EXISTENCE AND STABILITY OF TWO-CLUSTER STATES

We briefly summarize the existence and stability analysis of the two cluster states and the condition for the existence of attracting heteroclinic cycles between a pair of two cluster states.^{20,21} There is a family of two-cluster states in Eq. (23), in which qN_1 oscillators and $(1-q)N$ oscillators form point clusters. Let ϕ_A and ϕ_B be the phase of these clusters. The phase difference $\Delta\phi = \phi_A - \phi_B$ is obtained as the solution to

$$(2q-1)\Gamma(0) + (1-q)\Gamma(\Delta\phi) - q\Gamma(-\Delta\phi) = 0. \quad (\text{B1})$$

The eigenvalues of the corresponding stability matrix are

$$\lambda_1 = Kq\Gamma'(0) + (1-q)\Gamma'(\Delta\phi), \quad (\text{B2})$$

$$\lambda_2 = K(1-q)\Gamma'(0) + q\Gamma'(-\Delta\phi), \quad (\text{B3})$$

$$\lambda_3 = K(1-q)\Gamma'(0) + q\Gamma'(\Delta\phi), \quad (\text{B4})$$

with multiplicities $Nq-1, N(1-q)-1, 1$, respectively. There is also one trivial eigenvalue $\lambda_0 = 0$. Eigenvalues λ_1 and λ_2 are associated with intra-cluster fluctuation, and λ_3 is associated with inter-cluster fluctuation. For generic Γ , many of the two-cluster states are saddles, i.e., only a part of eigenvalues are negative. Nevertheless, such saddle states are meaningful because pairs of the two-cluster states form attracting heteroclinic cycles and the system may approach one of them. From here, for simplicity, we only consider two-cluster states with $q = \frac{1}{2}$. There are a pair of two-cluster states with the phase differences $\pm\Delta\phi$. The heteroclinic cycle can be formed between this pair of cluster states, if

$$\lambda_1 > 0, \quad \lambda_2 < 0, \quad \lambda_3 < 0. \quad (\text{B5})$$

Furthermore, the cycle can be attracting, if

$$\left|\frac{\lambda_1}{\lambda_2}\right| \leq 1. \quad (\text{B6})$$

The solid line in Fig. 7 is plotted in the following manner. For given Γ , Eq. (B1) is solved numerically to find $\Delta\phi$. Using this $\Delta\phi$ value, we check Eqs. (B5) and (B6). If both stability conditions are satisfied, we plot a R value given by Eq. (24) in Fig. 7.

¹A. T. Winfree, *The Geometry Of Biological Time* (Springer-Verlag, New York, 2001).

²Y. Kuramoto, *Chemical Oscillations, Waves, and Turbulence* (Springer-Verlag, Berlin, Heidelberg, 1984).

³A. Pikovsky, M. Rosenblum, and J. Kurths, *Synchronization: A Universal Concept In Nonlinear Sciences* (Cambridge University Press, 2001).

⁴H. Kori, Y. Kuramoto, S. Jain, I. Z. Kiss, and J. L. Hudson, "Clustering in globally coupled oscillators near a hopf bifurcation: Theory and experiments," *Phys. Rev. E* **89**(6), 062906 (2014).

⁵J. M. B. Amaral, M. Delmar, A. Vinet, D. C. Michaels, and J. Jalife, "Phase resetting and entrainment of pacemaker activity in single sinus nodal cells," *Circ. Res.* **68**(4), 1138–1153 (1991).

⁶R. Wessel, "In vitro study of phase resetting and phase locking in a time-comparison circuit in the electric fish, eigenmannia," *Biophys. J.* **69**(5), 1880–1890 (1995).

⁷S. B. S. Khalsa, M. E. Jewett, C. Cajochen, and C. A. Czeisler, "A phase response curve to single bright light pulses in human subjects," *J. Physiol.* **549**(3), 945–952 (2003).

⁸A. A. Prinz, V. Thirumalai, and E. Marder, "The functional consequences of changes in the strength and duration of synaptic inputs to oscillatory neurons," *J. Neurosci.* **23**(3), 943–954 (2003).

⁹I. Z. Kiss, Y. Zhai, and J. L. Hudson, "Predicting mutual entrainment of oscillators with experiment-based phase models," *Phys. Rev. Lett.* **94**(24), 248301 (2005).

¹⁰S. Koizumi, H. Kori, I. T. Tokuda, K. Yagita, and Y. Shigeyoshi, "Transition of phase response properties and singularity in the circadian limit cycle of cultured cells," *PLoS One* **12**(7), e0181223 (2017).

¹¹E. M. Izhikevich, *Dynamical Systems In Neuroscience* (MIT Press, 2007).

¹²Y. Kuramoto, "Collective synchronization of pulse-coupled oscillators and excitable units," *Phys. D* **50**(1), 15–30 (1991).

¹³L. F. Abbott and C. van Vreeswijk, "Asynchronous states in networks of pulse-coupled oscillators," *Phys. Rev. E* **48**(2), 1483 (1993).

¹⁴H. Kori, "Slow switching in a population of delayed pulse-coupled oscillators," *Phys. Rev. E* **68**(2), 021919 (2003).

¹⁵S. Olmi, A. Politi, and A. Torcini, "Collective chaos in pulse-coupled neural networks," *Europhys. Lett.* **92**(6), 60007 (2011).

¹⁶J.-M. Flesselles, A. Belmonte, and V. Gaspar, "Dispersion relation for waves in the Belousov-Zhabotinsky reaction," *J. Chem. Soc., Faraday Trans.* **94**, 851–855 (1998).

¹⁷I. Z. Kiss, Y. Zhai, and J. L. Hudson, "Emerging coherence in a population of chemical oscillators," *Science* **296**(5573), 1676–1678 (2002).

¹⁸I. Z. Kiss, Y. Zhai, and J. L. Hudson, "Characteristics of cluster formation in a population of globally coupled electrochemical oscillators: An experiment-based phase model approach," *Prog. Theor. Phys. Suppl.* **161**, 99–106 (2006).

¹⁹K. Okada, "Variety and generality of clustering in globally coupled oscillators," *Phys. D* **63**(3–4), 424–436 (1993).

²⁰D. Hansel, G. Mato, and C. Meunier, "Clustering and slow switching in globally coupled phase oscillators," *Phys. Rev. E* **48**(5), 3470 (1993).

²¹H. Kori and Y. Kuramoto, "Slow switching in globally coupled oscillators: Robustness and occurrence through delayed coupling," *Phys. Rev. E* **63**(4), 046214 (2001).

²²T. Chen, M. R. Tinsley, E. Ott, and K. Showalter, "Echo behavior in large populations of chemical oscillators," *Phys. Rev. X* **6**(4), 041054 (2016).

²³J. Lewi, R. Butera, and L. Paninski, "Sequential optimal design of neurophysiology experiments," *Neural Comput.* **21**(3), 619–687 (2009).

²⁴G. Bard Ermentrout and N. Kopell, "Parabolic bursting in an excitable system coupled with a slow oscillation," *SIAM J. Appl. Math.* **46**(2), 233–253 (1986).